JOURNAL OF PROPULSION AND POWER
Vol. 14, No. 6, November–December 1998

Numerical Model of Cesium Ion Beams in Field Emission Electric Propulsion Thrusters

Mariano Andrenucci*
University of Pisa, Pisa 56100, Italy
Alessandro Ciucci† and Salvo Marcuccio‡
Centrospazio, Ospedaletto, Pisa 56014, Italy
and
Giuseppe Barsotti§
University of Pisa, Pisa 56100, Italy

A numerical model of the ion beam in field emission electric propulsion thrusters is presented. The objective of the study is to develop a computational tool capable of predicting the effects of thruster configuration parameters (geometry, voltage distribution between the electrodes) on thruster performance (beam divergence, ion exhaust velocity). A two-dimensional, steady model has been adopted. A simple emission model has been assumed, neglecting the detailed, microscopic description of the physical emission mechanism. The electric field is evaluated by a finite element scheme; boundary conditions are provided by an auxiliary technique based on the placement of fictitious charges in proximity to the electrode surfaces. The beam is simulated through a discrete number of charged particles; the effects of the associated space charge density distribution on the electric field is considered. The results of the simulations of typical thruster configurations are presented and discussed. The need to take space charge effects into account to attain a sufficiently accurate solution is indicated: the beam charge density modifies the electric potential distribution generated by the electrodes voltage difference, causing a decrease in the local electric field at emitter tip and an increase in beam divergence. Neutralization at a finite distance must be taken into account to fully appreciate the effects of different voltage distributions between the electrodes: a higher accelerator electrode voltage determines a lower ion exhaust velocity and a larger beam divergence. The capability of an additional, decelerating neutral electrode to focus the ion beam is also investigated, showing that only little improvement in beam containment is attained.

Nomenclature

A = influence coefficient matrix
a = emitter–accelerator axial distance
b = accelerator slit half-width
I_e = total emission current
$\boldsymbol{J}$ = electric current density vector
j = dimensionless current density per unit arc length
l = transverse length of emitter slit
M = ion mass
$\boldsymbol{Q}$ = electric charges vector
q = ion electric charge
$\boldsymbol{r}$ = ion position vector
$\boldsymbol{U}$ = assigned voltage at control points
$\boldsymbol{U}_{ec}$ = electric potential at control points caused by emitted charges
$\boldsymbol{V}$ = ion velocity vector
V_a = accelerator electrode voltage
V_{add} = additional electrode voltage
V_e = emitter voltage
w = width of emitter slit
x_n = distance of neutralization line from emitter tip
x, y, z = Cartesian coordinates
α = beam azimuthal divergence angle
β = beam lateral divergence angle
ΔU = total applied voltage
ε_0 = vacuum electric permittivity
$\theta_{\max}$ = emision angular width
ρ_e = electric charge density
τ = parameter in emission model
ϕ = electric potential

Received Aug. 5, 1994; revision received Jan. 26, 1998; accepted for publication June 17, 1998.

*Professor, Department of Aerospace Engineering; Director, Centrospazio, Pisa, 56014 Italy. Member AIAA.
†Senior Engineer; currently at Centro Italiano Recerche Aerospaziali, Propulsion Section, 81043, Capua, Italy. Member AIAA.
‡Project Manager, FEEP Section. Member AIAA.
§Graduate Student, Department of Aerospace Engineering; currently Senior Engineer, Alitalia, Rome 00100, Italy.

Introduction

FIELD emission electric propulsion (FEEP) is an advanced electrostatic propulsion concept developed in Europe.[1] In a FEEP emitter, a liquid metal (usually cesium) flows into the slit between two metal blades under the action of capillary forces. Figure 1 shows a photograph of the emitter. The free surface of the liquid metal at the emitter tip assumes a near cylindrical shape, with a radius of curvature in the order of 1 μm. In this configuration, the application of a voltage difference of about 10 kV between the emitter and an accelerator electrode (Fig. 2) results in the onset of local instabilities of the liquid metal surface because of the combined effects of surface tension and electrostatic field, which leads to the formation of the protrusions known as Taylor cones. If the electric field is raised above a threshold value, liquid metal atoms are ionized and accelerated away. Specific impulse is in the order of 10^4 s. The thruster must be equipped with a neutralizer, which prevents the buildup of electrostatic charge on the vehicle and stalling of the beam.

Previously intended for attitude control and north-south station keepsing (NSSK) of small satellites, FEEP thrusters have

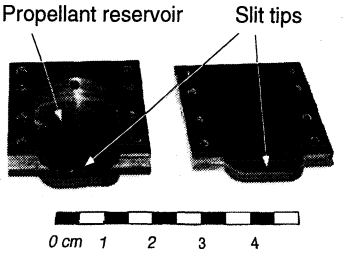

Fig. 1 FEEP emitter.

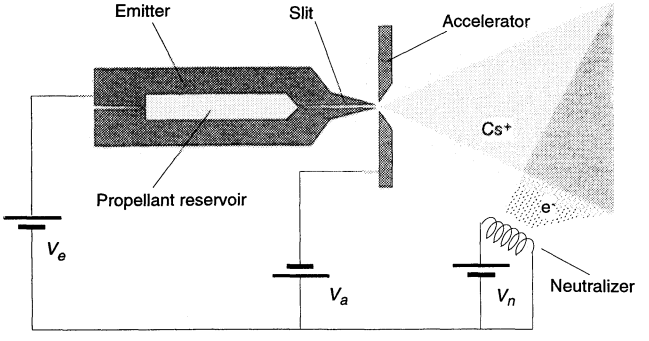

Fig. 2 Schematic of FEEP thruster assembly.

gained considerable attention as the ideal candidate for disturbance compensation systems on scientific spacecraft because of their excellent operational characteristics in the micronewton thrust range.[2,3] Presently, the FEEP system components (thruster, feeding system, neutralizer, power conditioning unit) are being down-scaled from the existing mN thrust level hardware to meet the needs of the μN system. Application of these thrusters as high-performance drag-free controllers for scientific spacecraft would result in considerable advantages from both weight and performance standpoints. While the intrinsic high specific power (about 50 W/mN) of FEEP thrusters may be a disadvantage when a mN thrust is required, it poses no problem at the μN level. In this thrust range, FEEP features unique controllability, resolution, and ease of operation; moreover, the absence of moving parts eliminates the concern for mechanical/gravitational disturbances in a delicate microgravity environment.[4,5]

This paper describes the techniques used and the results obtained from a computational study aimed at the numerical modeling of FEEP thrusters. The objective of this study was the development of a computational tool capable of predicting the effects of thruster configuration parameters (geometry, voltage distribution between the electrodes) on thruster performance (beam divergence, exhaust ion velocity). The process of thruster optimization for a given propulsion task is greatly simplified if experimental testing is preceded by a computational investigation. Moreover, a numerical simulation can help investigate the shape of the ion beam and the associated current distribution, which provides useful indications for thruster/spacecraft integration.

Computational studies of a linear slit emitter configuration were carried out in the late 1970s.[6] The model accounted for such effects as space charge and neutralization; however, in these early studies the solution presented limited accuracy in the high gradient regions, as a boundary condition update was not included in the iteration scheme. More recently, axisymmetric geometries were investigated to assess the potential benefits of annular-slit emitters.[7] Although very attractive from a performance standpoint, axisymmetric-slit emitters are currently not being considered, due to the inherent difficulties in the manufacturing process. However, the model employed in this case presented several improvements with respect to earlier models because it was based on an iteration procedure that significantly increased accuracy.

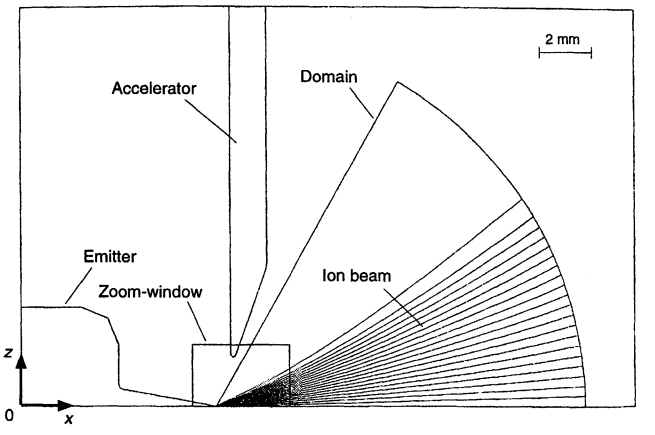

Fig. 3 Typical thruster configuration.

The mathematical model and the numerical techniques presented in this work are based on the model employed in axisymmetric geometry, with the governing equations properly formulated in a two-dimensional, Cartesian reference frame. Several aspects were improved or added, such as an increased flexibility in handling the boundary conditions and in taking into account neutralization effects, an improved ion emission model, and an increased capability for easily varying the geometry, to provide a useful tool for preliminary design and parametric analyses.

Model

Governing Equations

The analysis of the electric field around the thruster and of the trajectories of the emitted ions is performed assuming a steady, two-dimensional model, considering a domain in the x–z plane of symmetry of the emitter. A schematic of a typical thruster configuration and of the domain assumed for most calculations performed in this study is shown in Fig. 3. The assumption of a two-dimensional model to simulate a linear geometry of finite length implies that side effects at the edges of the emitter slit need not be included in the model. Thus, the effects of the lateral (β) divergence of the beam on thruster performance should be accounted for separately; however, such a contribution is known to be very small.[8] Furthermore, a detailed, microscopic physical description of the emission process is not considered, in accordance with the macroscopic nature of the present model. The domain is represented by an annulus sector with its center at the emitter tip, the inner circle being located very close to the emitter and the outer boundary extending to the region where either neutralization takes place or the electric field becomes so weak that the ion trajectories can be reasonably approximated as straight lines.

The electric field can be determined by solving the following Poisson equation for the electric potential ϕ:

$$\nabla^2\phi = -(\rho_e/\varepsilon_0) \tag{1}$$

where ρ_e is caused by the emitted ions. The electric current conservation law for the ion beam and the assumed relation between current and charge density are expressed as

$$\nabla\cdot\boldsymbol{J} = 0 \tag{2}$$

$$\boldsymbol{J} = \rho_e\boldsymbol{V} \tag{3}$$

The ion trajectories are evaluated for a discrete number of particles from the solution of the following equation of motion for the ions:

$$M\ddot{\boldsymbol{r}} = q\nabla\phi \tag{4}$$

where M and q are the mass and electric charge of an ion, respectively, and $\boldsymbol{r}$ indicates its position in space. Only singly ionized particles are considered. With this approach the beam is simulated using a finite number of charged particles. This allows the evaluation of the trajectories in the discrete scheme, with a substantial simplification of the governing equations, but retaining a satisfactory level of accuracy.

Therefore, in the continuum/particulate approach of the present model, Eqs. (1–4) represent a set of governing equations in the four unknowns ϕ, $\boldsymbol{J}$, ρ_e, and $\boldsymbol{V}$, which fully define the electric field and the ion trajectories in the region of interest.

Boundary Conditions

The governing equations can be solved upon specification of the appropriate boundary conditions at all required boundaries of the domain. These conditions are usually not known a priori, as the four sides of the domain are represented by free surfaces in a region near the two electrodes. In particular, the Poisson equation for the electric potential ϕ requires that suitable boundary conditions, in Dirichlet or Neumann form, be supplied on the closed contour delimiting the domain; in this study, the value of ϕ on the boundary is assigned through an auxiliary technique usually referred to as the charge substitution method (CSM). Also, the initial position and velocity of the ions must be specified at the inlet boundary to calculate the motion of the particles; these values are determined from the model of the emission process and the conservative nature of the electric field. The CSM and the model assumed for the ion emission are discussed in more detail in the following text.

CSM

The aim of this method is to obtain suitable boundary conditions for the solution of Eq. (1). According to the superposition principle, the value of the electric potential at any one point is obtained by expressing the solution to the linear differential equation [Eq. (1)] as a linear combination of simpler (known) solutions corresponding to elementary charge distributions. The potential field generated by the actual voltages applied to the electrodes in the configuration being examined is reproduced by distributing (unknown) fictitious charges at suitable collocation points inside the electrodes. The magnitude of these electric charges is determined by requiring that, as a result of the combined effect of all charges at the collocation points, the value of the electric potential at chosen control points on the electrodes surface be equal to the known applied voltage. By choosing the same number of fictitious charges and control points, the formulation leads to the following set of linear, algebraic equations:

$$A\boldsymbol{Q} = \boldsymbol{U} + \boldsymbol{U}_{ec} \tag{5}$$

where A is the influence coefficient matrix, whose elements a_{ij} represent the value of the electric potential at control point j caused by a unitary fictitious charge placed at collocation point i; $\boldsymbol{Q}$ is the vector of the unknown electric charges; $\boldsymbol{U}$ is the vector of the known voltage at the control points, and $\boldsymbol{U}_{ec}$ is the value of the potential at the same points because of the distribution of actual emitted charges (ion beam). In this work, each unknown electric charge is represented by a uniform charge distribution on a line segment both symmetric and perpendicular to the x–z plane. Once the magnitude of the charges, $\boldsymbol{Q}$, is determined, the value of the electric potential at a generic point k (and, thus, also at a point on the domain boundary) is calculated from the superposition of the potential because of all charges (fictitious and real) in the field as

$$U_k = \sum_i \alpha_{ki} Q_i + U_{ec} \tag{6}$$

a_{ki} being the influence coefficient between points k and i, and U_{ec} representing the contribution of the actual emitted charges. An analogous relation can be written for the three components of the electric field at point k.

Alternatively, the CSM could be employed to compute the solution in the entire domain considered, and not just on its boundary. However, considering the low level of accuracy achieved with this method, particularly in high gradient regions, the use of dedicated solution techniques such as finite difference methods or finite element methods is strongly recommended, and is the approach adopted for this study.

Emission Model

The integration of the equation of motion and the evaluation of the space charge density requires the specification of the initial position and velocity of the emitted particles and the distribution and magnitude of the total emitted current. These, in turn, depend on the physical processes occurring locally during emission, which would require the microscopic modeling of such phenomena as the deformation of the liquid surface and its development into an emitting source shaped like a Taylor cone,[9] and the distribution of the emitting sites along the emitter slit.[10] However, such detailed microscopic modeling was beyond the scope of the present work, especially considering the complexity of the phenomena involved. Therefore, a macroscopic approach was adopted, assuming that the emission of charged particles takes place from a hemicylindric surface close to the emitter tip, specifically from points located on an arc ranging from the centerline to an angular position θ_{max} and having a radius equal to the slit half width (Fig. 4a);

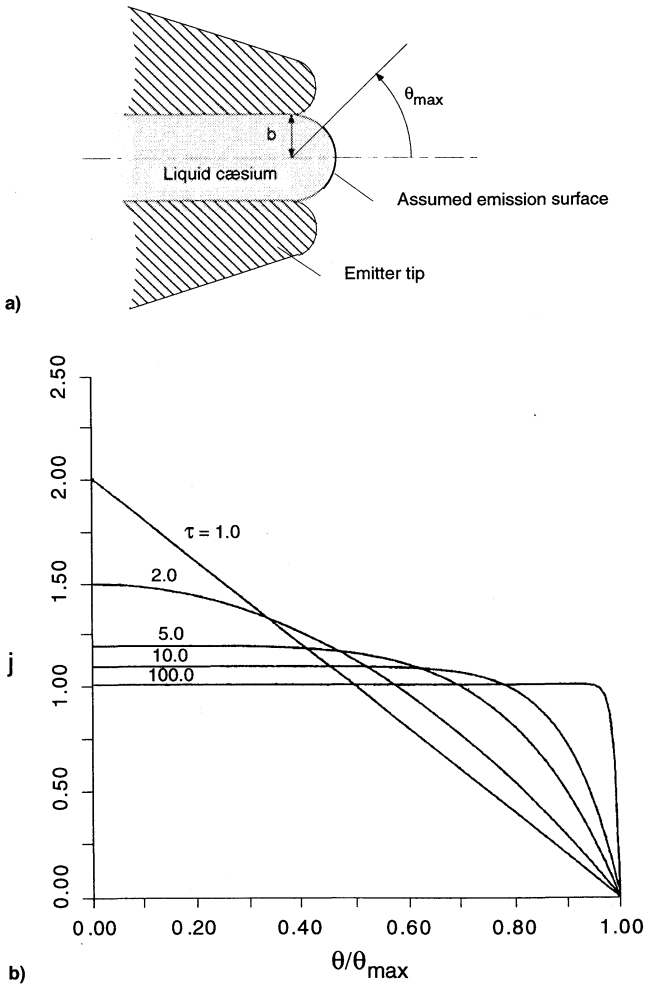

Fig. 4 a) Schematic representation of assumed emission surface geometry; b) distribution of dimensionless current density along the inner arc of the mesh.

ion emission has a continuous distribution on the specified arc length (in the circumferential direction) and, consistently with a two-dimensional model, remains constant in the transverse y direction (along the emitter slit). This assumption is well justified by the high density of emission sites.[11]

The ions are released with zero velocity. Conditions on the inner arc of the domain (inflow boundary) are determined assuming that the ion trajectories between the emitter tip and this inner arc are straight lines, and recognizing that the electric field is conservative. Velocity is assumed to be directed along radial lines. This approach is in accordance with all the other simplifying assumptions made on the emission process.

The distribution of the electric current density j associated with the ion beam is assigned on the inner boundary of the domain and is characterized by a parameter τ, which identifies a distribution function from a given family of curves:

$$j(\xi) = [(\tau + 1)/\tau](1 - \xi^{\tau}) \tag{7}$$

with $\xi = \theta/\theta_{\max}$. This distribution is shown in Fig. 4b. In addition, the value of the total emission current per unit (transverse) length of the thruster, I_e/l, must be given.

Hence, the characteristics of the emission model employed in this study are defined completely through the three parameters $\theta_{\max}$, τ, and I_e/l; these parameters are derived from experimental data available for linear FEEP thrusters.[12–14] The experimental measurements are also employed to define an empirical relation between the electric current per unit length and characteristic quantities such as the slit width and the local electric field in the proximity of the emitter tip; thus, the correct value of I_e/l can be estimated for thruster configurations different from the current one. The values of $\theta_{\max}$ and τ, on the other hand, are assumed to remain the same in other configurations. Further details on the emission model can be found in Ref. 15.

Procedure

The set of governing equations [Eqs. (1–4)], with boundary conditions given by Eq. (6) and as specified by the emission model, is solved numerically through the following iterative scheme:

1) The CSM is applied to determine ϕ on the domain boundary with no emitted charge; the Laplace equation, obtained from Eq. (1) with $\rho_e = 0$, is then solved, thus providing a first approximation for the electric potential.

2) The equation of motion [Eq. (4)] is integrated for a discrete number of ions.

3) The local charge density, ρ_e, is obtained from Eqs. (2) and (3).

4) The CSM is applied again, taking the effects of the emitted charge distribution into account. The Poisson equation is solved using the known values of ρ_e to obtain a new estimate of the electric potential.

The preceding steps are then repeated until convergence, in terms of ϕ, is achieved. Each equation is solved through an appropriate numerical technique that is briefly described in the following text.

Finite Element Method

The finite element method (FEM) is adopted for the solution of the Poisson equation. This numerical technique was preferred to other schemes such as finite difference methods because of its greater accuracy and flexibility for the problem at hand. The mathematical problem leads to a variational formulation in terms of minimization of the function representing the total potential energy per unit length of the electrostatic field. The domain is divided into subdomains, or elements, through a certain number of radial and circumferential lines; the grid becomes finer moving toward the emitter tip because the electric field gradient is higher in this region. A typical grid is shown in Fig. 5.

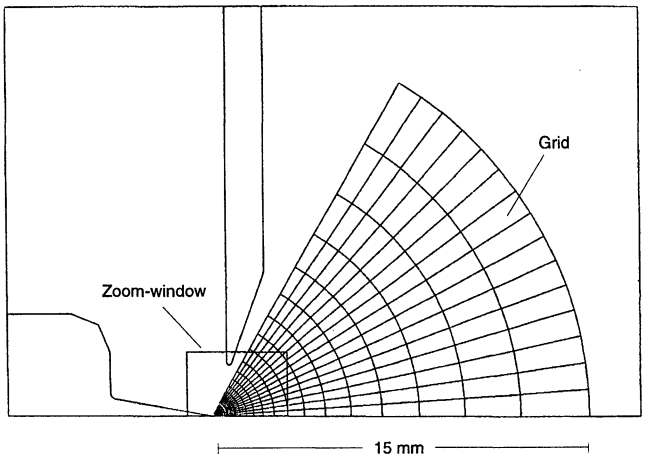

Fig. 5 Computational grid.

Elements having four, eight, or nine nodes, along with different shape functions, can be employed, according to the degree of accuracy required. This formulation leads to the solution of a set of algebraic equations, which determines the value of the electric potential at the nodes. The value of ϕ at any other point of the domain is computed through the shape functions. The details of the analytical development of the method are omitted here for brevity; considerable documentation on the subject is available in the literature.[16,17]

Ion Trajectories

Once an estimate of the electric field has been obtained with the FEM, the ion trajectories are determined through the solution of Newton's second law [Eq. (4)], projected accordingly along the two coordinate axis x and z, employing the boundary conditions derived from the emission model. The numerical method adopted for the solution of Eq. (4) is based on Milne's predictor–corrector method.

Space Charge Density

After the trajectories and velocities of the emitted particles have been determined, the associated space charge density can be calculated from Eqs. (2) and (3). Applying the electric current density conservation law, in integral form, to each stream tube defined by two adjacent trajectories, and assuming a one-dimensional flow in the tube, the charge density ρ_e is evaluated from the known ion velocity and the assumed current density on the inflow boundary of the domain. The value obtained is assigned to the midpoint of the line segment representing the outflow of the stream tube. The charge density at the nodes is then calculated through interpolation, and the value at any point inside the domain through the shape functions.

The contribution of the actual electric charges to the electric potential U_{ec} at a generic point, as required in the subsequent application of the CSM, can be found from the estimated value of ρ_e. The potential at a point $P_0(x_0, z_0)$, resulting from the charge distribution in element m of the mesh, is obtained from

$$U_{ec} = \int_A \rho_e(x, z) F(x, z, x_0, z_0, l)\, \mathrm{d}A \tag{8}$$

where ρ_e is at point $P(x, z)$ of element m, A is the area of the element, and F is the electric potential at P_0 because of a unitary charge distributed on a line segment placed in P. This integral is calculated performing a coordinate transformation in which each element of the mesh in the x, z plane is transformed into a unit square in the ξ, η plane, and then applying a Gauss–Legendre quadrature.

Neutralization

An important feature of the present model is represented by its capability to account for the effects of the neutralization process. The correct operation of an electrostatic thruster producing thrust through the emission of charged particles (positive ions) requires that other particles with opposite charge (electrons) be ejected downstream of the electrodes, to produce a globally neutral beam. This requirement originates from the need to prevent electrical charging of the spacecraft and to avoid stalling of the ion beam. The presence of neutralization substantially affects thruster performance, as the results presented in this paper will show.

Although the neutralization process may be quite complex, a detailed description of the phenomena occurring in the region of particle mixing is not required. A general analysis of neutralization and its application to electrostatic engines has been presented by Jahn.[18] In this work, neutralization is simulated through a zero-potential line downstream of the accelerating electrode; in particular, an arc of circumference that is concentric with and has the same angular width as the computational domain has been adopted. This arc may coincide with the outflow boundary of the domain itself or be placed downstream of it, and should roughly simulate the location of the electron injection region in a real system.

The electron trajectories are not integrated, and their effects on the charge distribution are modeled by assuming a space charge density that decreases linearly along a radial direction from its value on the domain outflow boundary to zero at the neutralization line; the charge density is set to zero downstream of this line. If the neutralization line coincides with the outflow boundary, then ρ_e is assumed to decrease to zero from the second to the last circumferential line of the mesh. Because the evaluation of the electric field and the ion trajectories in the region between the domain and the neutralization line is not required to calculate the charge density, the position of this line can be chosen independently from the dimensions of the domain. However, with regard to thruster performance predictions, the distribution of position and velocity of the ions at the neutralization line must be known. These are obtained by extrapolating the trajectories from the domain exit contour to the neutralization line by simply assuming a uniform rectilinear motion for the ions; this assumption is acceptable provided that the neutralization line is placed downstream of the mesh exit at a distance sufficient to keep the electric field at a low level in this region. As far as the CSM is concerned, the simulation of the zero-potential line is carried out by treating it as a virtual electrode; unknown electric charges, placed at collocation points slightly downstream of the neutralization line, are determined by requiring that the potential determined by all charges at control points on this line be zero. Finally, it should be noted that the ideal case in which neutralization takes place at an infinite distance (a condition nearly attained in a vacuum chamber during laboratory testing) can be simulated simply by placing a line at a large, but finite, distance from the thruster electrodes, to take into account the charge density between the domain exit contour and this line. The effects caused by the space charge outside this region are very small and thus negligible.

Results and Discussion

A preliminary validation of the computer program was carried out to check convergence and accuracy of the solution.[15] Several model parameters, which were seen to affect the solution to some extent, were systematically varied and optimized, including the kind of mesh adopted, the type of element and shape function in the FEM, the choice of the location of control and collocation points in the CSM, and the length of the line segment over which the fictitious charges are distributed. A study of the grid influence on the solution was performed, including variation of the mesh angle and of the mesh extension (location of both inlet and outlet boundaries). Eight-node quadrilateral elements, with a biquadratic Lagrangian polynomial as the shape function, were chosen for all computations. This is the most effective choice because the eight-node elements, compared with the four-node elements, permit a higher rate of convergence and an improved accuracy with the given grid; alternatively, a much finer grid should be used with four-node elements to achieve the same accuracy level obtained with eight-node elements. The number of grid points was progressively increased until no significant changes in the solution were observed. The computational grid finally adopted has a 60-deg angle, an inner and outer radii of 0.1 and 15 mm, respectively, and a total number of 26 × 16 grid points. After the final configuration of the model and computer code was established, several test-cases were analyzed; in all cases, convergence was quickly achieved in five or six iterations with a satisfactory degree of accuracy.[19] A selection of the most representative cases, illustrated in Table 1, is presented. In all of these test cases, the values adopted for the emission parameters are $\theta_{max} = 40$ deg, $\tau = 2$, and $I_e/l = 0.4$ mA/mm. A relative comparison of these results allow some preliminary conclusions on thruster configuration and performance to be drawn.

Table 1 Test classification

Test case no.	Emitter voltage kV	Accelerator voltage, kV	Voltage applied to additional electrode, kV	Distance of neutralization line from emitter tip, mm
1	8	−4	——	∞
2	6	−6	——	∞
3	8	−4	——	30
4	6	−6	——	30
5	2	−10	——	30
6	8	−4	0	∞

Reference Emitter–Accelerator Configuration

The first case analyzed was the typical emitter–accelerator base configuration in the absence of a neutralizer, i.e., assuming that neutralization takes place at an infinite distance; this condition is very similar to that occurring during ground tests in a vacuum chamber. The emitter slit width, emitter–accelerator axial distance, and the accelerator slit half-width were assumed to be $w = 1$ μm, $a = 0.6$ mm, and $b = 2$ mm, respectively; these are typical values of an experimental thruster assembly. Case no. 1 was assumed as a reference case for comparison with all other cases investigated.

A three-dimensional representation of the distribution of the electric potential inside the domain is illustrated in Fig. 6. A projection on the x–z plane of the portions of the electrode profiles that were modeled and the outline of the mesh are also shown. The electric potential decreases very rapidly in the region near the emitter tip, indicating a very strong electric field that determines the emission and initial acceleration of the ions. Past the accelerator electrode plane, the value of ϕ continues to decrease at a lower rate until a minimum is reached; beyond this point, the potential gradually increases and tends to attain a zero value asymptotically at an infinite distance. A *saddle point* can be noted, where the minimum is reached along the x axis, denoting a zero value for the electric field. It should also be noted that the electric potential is not constant at the exit of the mesh, as it is nearly zero at the axis of symmetry but still has quite large negative values at the opposite end.

An electric potential contour plot is shown in Fig. 7, with 250-V equipotential line increments; their spacing provides a clear indication of the potential gradient, and thus of the intensity and direction of the electric field. Figure 8 shows the rectangle in Fig. 7, enlarged 5 times, with the details of the solution near the emission zone. An increase of the electric

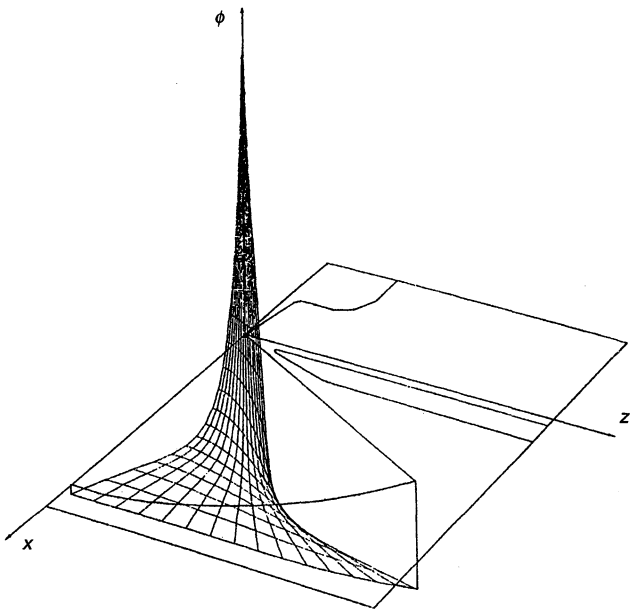

Fig. 6 Perspective representation of the electric potential distribution.

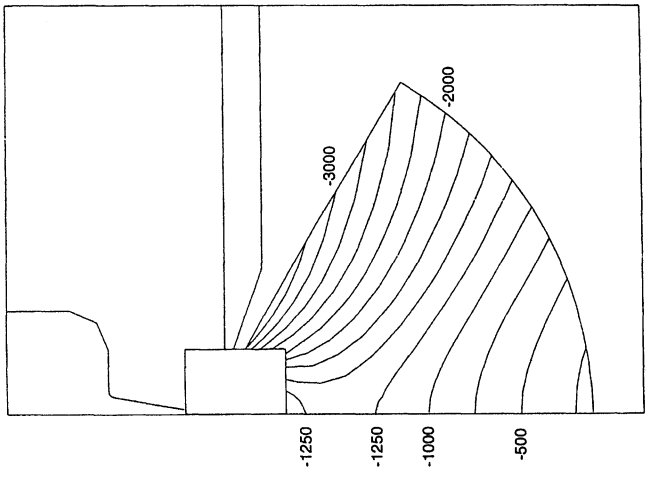

Fig. 7 Electric potential contours (case no. 1: V_e = 8 kV, V_a = −4 kV).

field near the emitter tip can be observed; also, note that the inflow boundary of the mesh is close to, but does not coincide with an equipotential line, thus indicating that the assumption that emitted particles enter the domain with zero circumferential velocity is only approximately correct. No appreciable variation in the solution is attained changing the position of the inlet boundary, unless the radius of the inner arc is decreased down to the value of approximately 1 μ, which would require unacceptably large computational resources. The ion trajectories are illustrated in Fig. 9; the electric field vector plot for the outer region of the domain is also shown. The beam was discretized by 21 particles, suitably spaced at the inlet boundary so that each stream tube determined by two adjacent particles carries the same fraction of the total current intensity, equal to 5% in this case. Thus, the picture of the beam gives a qualitative indication of its spreading and of the associated charge density distribution. The azimuthal divergence angle α, measured at the exit boundary of the mesh, is 42.5 deg, compared with the value of 40 deg assumed for $\theta_{\max}$ at the inlet boundary; hence, it would seem that the spreading of the ion beam is quite limited, and that the particles tend to move along radial straight lines. Most of the deviation takes

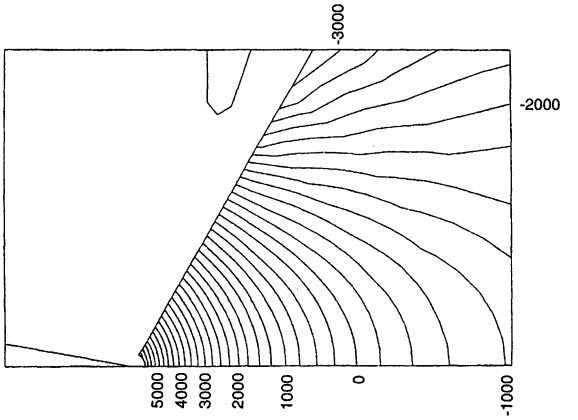

Fig. 8 Detail of equipotential lines (case no. 1: V_e = 8 kV, V_a = −4 kV).

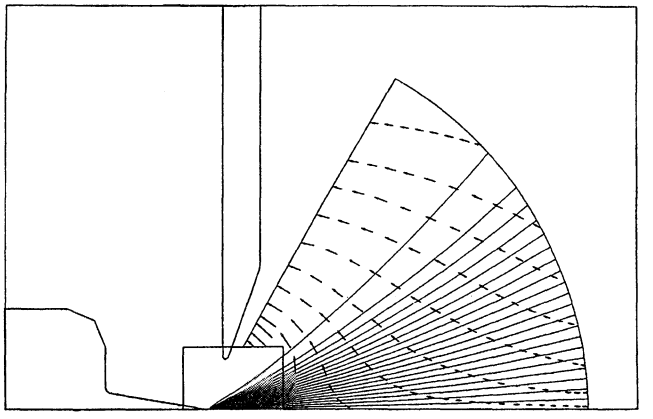

Fig. 9 Ion trajectories and electric field vectors (case no. 1: V_e = 8 kV, V_a = −4 kV).

place in the region past the accelerator plane and is more pronounced for the external particles.

The assessment of the effects of the space charge density distribution on the electric field and on the particle trajectories can be obtained by comparing the solution previously discussed with the results of the first iteration of the numerical scheme, in which the Laplace equation for the electric potential is solved (ρ_e = 0). This initial iteration provides the distribution of the potential when no emission (or emission with a very weak intensity) occurs. The results show that the main effect of a space charge distribution is an attenuation of the electric field close to the emitter tip, and an increase in the field strength in the region beyond the accelerator electrode, thus implying a higher azimuthal divergence angle. In Fig. 10, the electric potential distribution along the x axis of symmetry is illustrated for the two cases of no emission and of ion emission. Figure 11 shows the two trajectories comprising 50 and 100% of the total current intensity, relative to the first iteration (dashed lines) and to the converged solution (solid lines), respectively. The larger beam divergence caused by the space charge distribution is clearly evident. Therefore, the analysis of these results emphasizes the need of taking into account the charge density distribution to attain a realistic and sufficiently accurate solution.

Test case no. 2 refers to the same thruster configuration as the one adopted in the reference case, with the only difference that, for the same total voltage drop, ΔU, the electrode voltages were set to 6 and −6 kV for the emitter and the accelerator, respectively. The calculated results, in terms of electric field and ion trajectories, are quite similar to those obtained in case no. 1. As neutralization takes place in both cases at an infinite distance, a significant part of the ion deceleration occurs out-

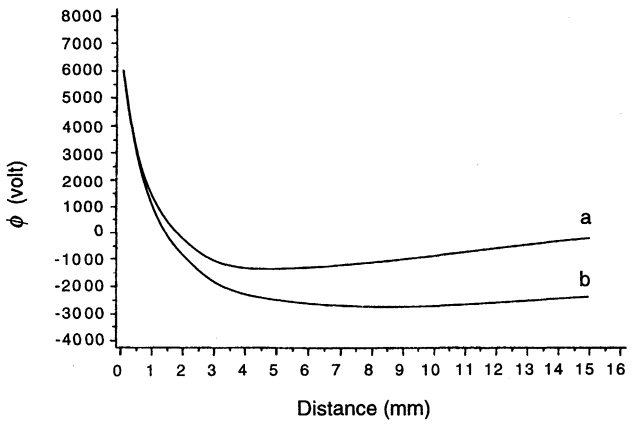

Fig. 10 Electric potential as a function of the distance from the emitter tip along the positive x axis: a) with space charge and b) without space charge.

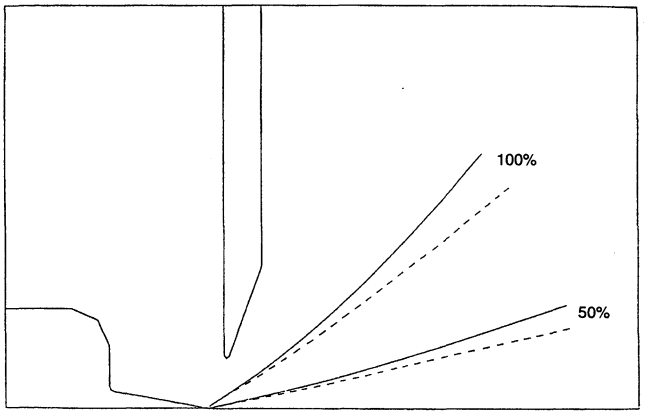

Fig. 11 Effects of space charge on beam divergence: comparison of ion trajectories comprising 50 and 100% of total current density (case no. 1: V_e = 8 kV, V_a = −4 kV): ——, converged solution; - - - -, first iteration.

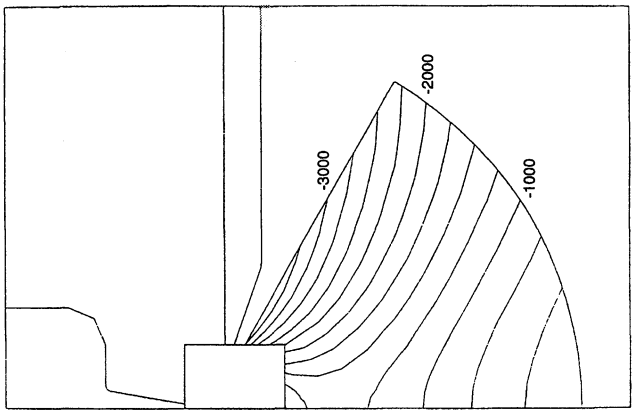

Fig. 12 Electric potential contours (case no. 3: V_e = 8 kV, V_a = −4 kV).

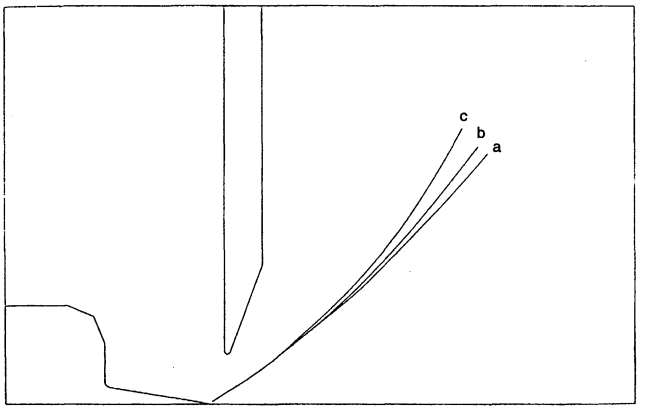

Fig. 13 Effects of neutralization on beam divergence, for different voltage distributions between the electrodes (ΔU = 12 kV). Ion trajectory comprising 100% of total current density for a) case no. 3: V_e = 8 kV, V_a = −4 kV; b) case no. 4: V_e = 6 kV, V_a = −6 kV; c) case no. 5: V_e = 2 kV, V_a = −10 kV.

side the mesh, in as much as the value of the electric potential at the outflow boundary is still quite different from the asymptotic value. Therefore, to obtain a realistic evaluation of the effects of the distribution of the potential between the electrodes, a neutralization surface at a finite distance from the emitting unit must be included in the model.

Neutralization at a Finite Distance

The effects of neutralization at a finite distance were examined in three different test cases, maintaining the same thruster geometry as in the reference case but adding a neutralization line at a distance x_n = 30 mm from the emitter tip. The three cases, no. 3, no. 4, and no. 5, differ only in the distribution of the same total electric potential between the two electrodes, given by 8/−4, 6/−6, and 2/−10 kV, respectively. A typical electric potential contour plot (8/−4 kV case) is shown in Fig. 12. In the rectangular region near the emitter tip (not shown) the differences among the three cases are very small; the accelerator electrode acts as a shield beyond which the presence of the neutralization line is not felt. This confirms that the distribution of the electric potential between the electrodes has a very weak influence on emission and initial acceleration of the ions, which depend only on the value of the total applied voltage ΔU, and on the local geometry of the thruster. In the outer region of the domain, external to the accelerator electrode, the solutions for the three cases are considerably different. Now the presence of the neutralization line forces the solution to a zero potential value; therefore, in going from case no. 3 to case no. 5, the spacing of the equipotential lines becomes progressively finer and, consequently, the intensity of the electric field increases, slowing down the ions and increasing the divergence of the beam. Figure 13 illustrates the beam divergence through the representation of the trajectories comprising 100% of the total current density for the three cases, no. 3–no. 5. As can be observed from this figure, the trajectories tend to approximate straight lines toward the exit of the mesh, indicating a proper choice of the neutralization line distance from the mesh exit. Hence, if on the one hand a smaller value of the emitter voltage reduces the exhaust velocity and, thus, the specific impulse and the specific power, on the other hand it also causes a larger beam azimuthal divergence angle.

It should be noted that, although the velocity at the exit of the mesh differs considerably in all three cases examined, the presence of a neutralization surface at a finite distance does not change the final value of velocity (at ϕ = 0), as compared with the value obtained with neutralization at infinite distance. In fact, the final velocity depends only on the value of the emitter potential. The position of the neutralization line, however, has a marked influence on how the final ion exhaust velocity is achieved, with shorter neutralization distances increasing electric field and velocity gradients, and beam divergence.

Decelerating Neutral Electrode

To assess the potential benefits of multielectrode configurations in terms of beam containment, a thruster geometry employing an additional electrode at zero potential, placed a short distance downstream from the accelerator, was investigated in test case no. 6. This neutral electrode should shield the ions in

the outer region from the attracting/deflecting effect of the accelerator. With respect to the reference case, the profile of the accelerator is inverted, its slit half-width reduced to b = 1.5 mm, and it is moved closer to the emitter tip. The additional, neutral electrode has the same profile as the accelerator but with a slit width of 6 mm, and is placed at a distance of 1 mm from it. All the other features are unchanged with respect to the reference case, including the emitter geometry, the voltages applied to the electrodes, and the emission parameters, with the exception of a reduction of the mesh angle to 52.5 deg, because of the smaller accelerator slit half-width. A schematic diagram of the thruster configuration for this case is shown in Fig. 14; the ion trajectories, calculated including the effects of the space charge density, are also shown.

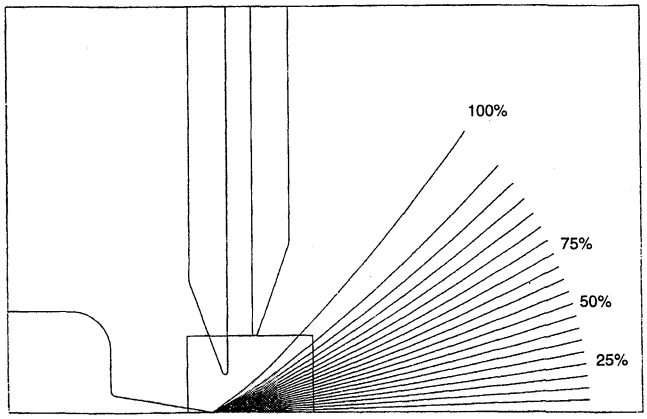

Fig. 14 Schematic of thruster configuration with neutral electrode and ion trajectories with values of comprised percentage of total current density (case no. 6: V_e = 8 kV, V_a = −4 kV, V_{add} = 0 V).

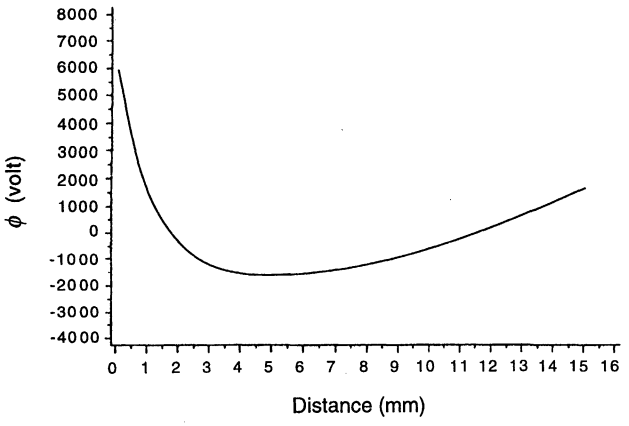

Fig. 15 Electric potential as a function of the distance from the emitter tip along the positive x axis with neutral electrode.

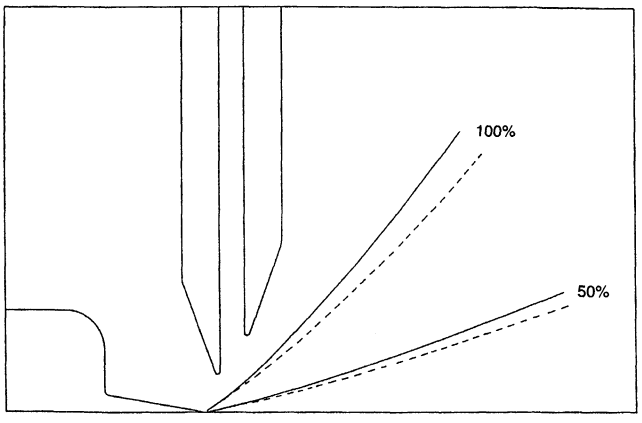

Fig. 16 Effects of neutral electrode on beam divergence: comparison of ion trajectories comprising 50 and 100% of total current density (case no. 6: V_e = 8 kV, V_a = −4 kV, V_{add} = 0 V): ——, with neutral electrode; - - - - without (case no. 2).

The results show that the equipotential lines in the inner region close to the emitter tip present a greater curvature and a finer spacing, thus denoting a stronger electric field than in the reference case. This is attributed to the accelerator electrode being closer to the emitter, as a given potential drop taking place over a shorter distance determines a higher electric field which, in turn, determines a higher emission and acceleration of the ions. On the other hand, the presence of the neutral electrode does not have any substantial effect on the field in this region. Again, the inflow boundary was moved closer to the emission surface, but only negligible differences in the solution were observed.

The electric field in the gap between the accelerator and neutral electrodes has a magnitude of about 4 kV/mm; this is well below the value at which an electric discharge is assumed to occur between the two conductors (about 10 kV/mm), thus assuring correct operation of the unit.

The electric field is rather strong in the region immediately beyond the accelerator electrode, causing a greater deviation of the particle trajectories than in the reference case. On the other hand, in the far field toward the exit of the mesh, the electric field is fairly weak, whereas the ion velocity is still high. It should be noted that the electric potential attains positive values at the outflow boundary, as shown in Fig. 15; thus, the deceleration of the ions is followed by an acceleration phase. If neutralization takes place at a finite distance, the electrons injected into the field would be accelerated toward the electrodes, thus altering the calculated charge density distribution and affecting somewhat the final solution. Because the motion of the electrons is not accounted for, this effect is not included in the model.

Hence, the addition of a neutral decelerating electrode downstream of the accelerator appears to be only of limited effectiveness in focusing the ion beam. The deflection of the trajectories is more localized between the accelerator and the neutral electrode, and the value of the divergence angle α has increased with respect to the reference case, as illustrated in Fig. 16. On the other hand, the relative position between emitter and accelerator appears to be of far more importance in determining the electric field.

Conclusions

A two-dimensional, steady model of the electric field and cesium ion beam associated with the operation of a linear FEEP thruster has been developed. The main purpose of the work is to develop a computational tool to investigate the effects of geometrical and operational parameters on thruster performance through a series of parametric studies. Such predictions should provide useful insights on the optimum thruster configuration with respect to its relevant performance requirements in terms of ion exhaust velocity, emission current level, beam divergence, and autofocusing capabilities. A selection of preliminary test cases directed at assessing the capability of the model to accurately simulate the electric field patterns and particle trajectories has been presented. The solution is obtained in a region close to the electrodes through the application of the FEM together with the CSM, and the integration of a discrete number of particle trajectories. Effects such as the emitted charge density, the distribution of the total applied voltage between the electrodes, and neutralization at a finite distance are accounted for in the model.

Despite the simplified, macroscopic modeling of emission and neutralization processes, some useful indications can be derived from the test cases examined. The electric charge density modifies the electric potential distribution, slightly reducing the intensity of the local electric field at the emitter tip, and increasing the beam azimuthal divergence angle. Neutral-

ization at a finite distance must be taken into account to correctly evaluate the effects of voltage distribution between the electrodes. The presence of a neutralization line does not affect the electric field distribution in the region close to the emitter tip appreciably; on the contrary, the electric field patterns and the motion of the ions are modified significantly in the outer field (with respect to the case of neutralization at infinite distance), with the result of an increased beam divergence. The closer the neutralization line to the electrodes, the stronger the effects on the field. The distribution of the total applied voltage between emitter and accelerator strongly affects thruster performance; a lower ion exhaust velocity (and thus a lower specific power) is attained by increasing the voltage applied to the accelerator electrode. Unfortunately, this favorable effect is accompanied by an undesired increase in beam divergence. Finally, it has been shown that the use of an additional, neutral electrode downstream of the accelerator does not change the field patterns significantly and, thus, does not result in any beneficial effect for the beam containment.

Despite its limitations, the present model represents a valuable tool that can be very useful in the optimization of a FEEP thruster configuration and operating conditions. A systematic comparison with the available experimental results must be carried out to further improve the current model. Moreover, additional investigations of the focusing capabilities of multielectrode configurations must be performed.

Acknowledgments

This work was performed under ESA Contract 6544/85/NL/PH through the European Space Research and Technology Center. Presented as Paper 93-154 at the 23rd International Electric Propulsion Conference, Seattle, WA, Sept. 13–16, 1993. The authors are indebted to G. Genuini for his invaluable contribution in the early definition of the computer program.

References

[1]Bartoli, C., Von Rohden, H., Thompson, S. P., and Blommers, J., "A Liquid Cæsium Field Ion Source for Space Propulsion," *Journal of Physics D: Applied Physics*, Vol. 17, 1984, pp. 2473–2483.

[2]Andrenucci, M., Marcuccio, S., and Genovese, A., "The Use of FEEP Systems for Micronewton Thrust Level Missions," AIAA Paper 93-2390, June 1993.

[3]Nobili, A. M., et al., "Galileo Galilei—GG: Flight Experiment on the Equivalence Principle with Field Emission Electric Propulsion," *Journal of the Astronautical Sciences*, Vol. 43, No. 3, 1995, pp. 219–242.

[4]Klotz, H., Strauch, H., Wolfsberger, W., Marcuccio, S., and Speake, C., "Drag-Free, Attitude and Orbit Control for LISA," *Proceedings of the ESA/ESTEC 3rd International Symposium on Spacecraft Guidance, Navigation and Control*, European Space Agency, Noordwijk, The Netherlands, 1996, pp. 695–702 (ESA SP-381).

[5]Marcuccio, S., Genovese, A., and Andrenucci, M., "FEEP Thrusters: Development Status and Prospects," *Proceedings of the 2nd European Spacecraft Propulsion Conference*, European Space Agency, Noordwijk, The Netherlands, 1997, pp. 149–153 (ESA SP-398).

[6]Thomas, C. L., et al., "Field Emission Electric Propulsion: Ion Optics of Slit Emitters and Beam Focussing," Final Rept. to ESTEC, Contract 3686/78, Culham Lab., Abingdon, UK, 1980.

[7]Andrenucci, M., Genuini, G., and Laurini, D., "Development of an Annular Slit Ion Source for Field Emission Electric Propulsion," AIAA Paper 85-2069, Sept. 1985.

[8]Bartoli, C., "A Review of Past and Present Studies on Ion Field Emission," *Proceedings of the ESTEC Field Emission Day*, European Space Agency, Noordwijk, The Netherlands, 1977, pp. 1–10 (ESA SP-119).

[9]Taylor, G., "Disintegration of Water Drops in an Electric Field," *Proceedings of the Royal Society of London*, A280, 1964, pp. 383–397.

[10]Prewett, P. D., "Liquid Metal Field Emission Thrusters and Ion Sources," Final Rept. to ESTEC, Contract 4462/80, Culham Lab., Abingdon, UK, 1983.

[11]Mitterauer, J., "Field Emission Electric Propulsion Spectroscopic Investigations on Slit Emitters," Final Rept. to ESTEC, Contract 5051/82, Vienna Technical Univ., Vienna, Austria, 1985.

[12]Ciucci, A., Andrenucci, M., and Genuini, G., "Experimental Investigation of Field Emission Electrostatic Thrusters," *Proceedings of the 22nd International Electric Propulsion Conference*, Viareggio, Italy, 1991 (IEPC-91-104).

[13]Genovese, A., Marcuccio, S., De Sio, M., and Andrenucci, M., "Pulsed FEEP: New Experimental Results," *Proceedings of the 24th Electric Propulsion Conference*, Moscow, Russia, 1995, pp. 643–648 (IEPC-95-97).

[14]Marcuccio, S., Genovese, A., and Andrenucci, M., "Experimental Performance of Field Emission Microthrusters," *Journal of Propulsion and Power*, Vol. 14, No. 5, 1998, pp. 774–781.

[15]Barsotti, G., "Modellizzazione e studio di propulsori FEEP in configurazione accel/decel," MS Thesis, Dept. of Aerospace Engineering, Univ. of Pisa, Pisa, Italy, 1987.

[16]Zienkiewicz, O. C., *The Finite Element Method*, McGraw–Hill, New York, 1977.

[17]Grandin, H., Jr., *Fundamentals of the Finite Element Method*, Macmillan, New York, 1986.

[18]Jahn, R. G., *Physics of Electric Propulsion*, McGraw–Hill, New York, 1968.

[19]Andrenucci, M., and Barsotti, G., "Field Emission Electric Propulsion: Preliminary Calculation of Ion Beam Trajectories in the Accel/Decel Configuration," Final Rept. to ESTEC, Contract 6544/85, Dept. of Aerospace Engineering, Univ. of Pisa, Italy, 1988.